# Spatial Dissipative Solitons in Graphene-Based Active Random Metamaterials

Ashis Paul,[1,*] Andrea Marini![](),[2,†] and Samudra Roy[1,‡]

[1]*Department of Physics, Indian Institute of Technology Kharagpur, West Bengal 721302, India*
[2]*Department of Physical and Chemical Sciences, University of L'Aquila, Via Vetoio, L'Aquila 67100, Italy*

We investigate dissipative nonlinear dynamics in graphene-based active metamaterials composed of randomly dispersed graphene nanoflakes embedded within an externally pumped gain medium. We observe that graphene saturable nonlinearity produces a subcritical bifurcation of nonlinear modes, enabling self-organization of the emitted radiation into several dissipative soliton structures with distinct topological charges. We systematically investigate the existence domains of such nonlinear waves and their spatial dynamics, finding that soliton vortices are unstable, thus enabling self-organization into single dissipative structures with vanishing topological charge, independently of the shape of the graphene nanoflakes. Our results shed light on self-organization of coherent radiation structures in disordered systems and are relevant for future cavity-free lasers and amplifier designs.

## I. INTRODUCTION

Dissipative solitons (DSs) are self-organized localized structures arising in diverse dissipative physical and biological systems [1], playing a central role in mode-locked lasers [2,3], photonic molecules [4], time-delay feedback systems [5], Bose-Einstein condensates of exciton polaritons [6], and cold atoms [7,8]. Conventional soliton families in nonlinear (NL) Hamiltonian systems arise from the delicate balance between dispersion and nonlinearity. Conversely, DSs ensue in nonintegrable systems due to the double balance of dispersion versus nonlinearity and NL gain versus NL loss [9]. In turn, DSs typically exist as isolated fixed-point solutions in the parameter space. Furthermore, DSs offer an appealing platform for cavity-free stimulated emission of radiation, as in particular in optical amplifiers [10]. In this context, innovative cavity-free radiation sources can be achieved also in colloidal solutions embedding randomly arranged scatterers and an optically active medium [11–13]—the so-called random lasers (RLs). However, cavity-free stimulated emission of radiation in RLs implies poor quality of the output beam, which inherently lacks reproducibility and tunability.

Recently, the advent of nanophotonic materials has enabled plasmon stimulated emission in metallic nanoparticles [14–16] and waveguides embedding gaining media [17–20]. Metamaterials (MMs) constitute a promising platform for planar sources of coherent radiation [21]

and for cavity-free lasers operating in the stopped-light regime [22,23]. Furthermore, MMs embedding subwavelength randomly arranged nanostructures in an amplifying medium are promising for achieving self-organized stimulated emission [24], enabling to control the properties of the output beam thanks to stable DSs. This requires the engineering and exploitation of the MM effective nonlinear optical response, which is greatly facilitated by graphene [25–27] because it provides saturated absorption (SA) at low peak intensities $\simeq$ MW cm$^{-2}$ [28–31] over a broad spectrum spanning the optical and infrared frequency ranges. This peculiar property of graphene is enabled by its conical band structure providing resonant interband absorption at arbitrary radiation frequencies, thus greatly facilitating the engineering of the random MM effective nonlinear response [24]. Indeed, graphene is ideal in versatile ultrafast pulsed fiber lasers [28] to produce mode-locked and *Q*-switched pulses [31]. Furthermore, graphene-based MMs provide an ideal platform for manipulating the propagation and the detection of terahertz waves [32] and to produce near-perfect light absorption in critically coupled resonators [33].

Here, we investigate the dissipative dynamics of nonlinear waves emitted in a realistic MM composed of disordered graphene nanoflakes embedded in externally pumped rhodamine 6G (R6G). Our model, accounting nonperturbatively for the saturable absorption of graphene nanoflakes and for the saturable gain of R6G, is based on an effective nonlinearly saturated propagation equation for the field envelope of the seeded radiation.

We observe that homogeneous nonlinear waves (HNWs) bifurcate from the trivial background subcritically and that

---
*apaul@phy.iitkgp.ac.in
†andrea.marini@univaq.it
‡samudra.roy@phy.iitkgp.ac.in

are bistable in a particular range of the linear gain coefficient. We further investigate HNW modulational instability, calculating the modulation gain spectrum, which suggests that DSs can be excited in the system. In turn, we investigate numerically DS existence, finding DS vortices with topological charges $m = 0, 1, 2$ and determining their existence domains. We also investigate DS stability over propagation, finding that only the $m = 0$ DSs can be stable in a well-determined range of the linear gain coefficient. Our results extend previous $(1 + 1)D$ investigations [24] shedding light to nonlinear dynamics in $(2 + 1)D$ and indicating that DSs offer a viable platform to manipulate the spatial pattern of the radiation seeded in random active MMs. Finally, we numerically investigate the collision dynamics of one DS pair (with $m = 0$) finding that, depending on the collision angle, the soliton pair either experiences an elastic collision or breaking into multiple localized structures. The observed DSs enable modal manipulation in cost-effective cavity-free lasers thanks to self-organization. Indeed, typical lasing devices require sophisticated designs and engineering of the photonic materials adopted. Conversely to standard MMs composed of ordered assemblies of subwavelength inclusions, graphene-based active random MMs do not require advanced micro- and nanofabrication techniques, thus implying lower cost and advanced design flexibility.

## II. MODEL

We consider a disordered medium, schematically depicted in Fig. 1, composed of undoped graphene nanoflakes (with lateral dimensions $<50$ nm) dispersed in polymethyl methacrylate (PMMA) embedding optically pumped R6G dyes, a typical gaining medium for RLs, see, e.g., Ref. [34]. The practical fabrication of our proposed disordered medium can be possible by dispersing the undoped graphene flakes in solutions such as dimethylformamide (DMF), which also dissolves R6G and PMMA. We also remark that a two-dimensional layered material such as graphene can be synthesized from graphite either by mechanical exfoliation [35] or chemical vapor deposition [36]. Population inversion in R6G can be attained by a frequency-doubled Nd-YAG laser-pump beam with wavelength $\lambda_{\text{pump}} = 532$ nm, providing peak stimulated emission at $\lambda_{\text{seed}} = 593$ nm. In turn, owing to the deep subwavelength dimensions of graphene nanoflakes, radiation seeded in such a system experiences an effective dissipative and nonlinear dielectric response arising from electron dynamics in graphene nanoflakes, PMMA and R6G.

PMMA acts as a background dielectric with relative permittivity $\epsilon_b \simeq 2.23$. In order to obtain the effective permittivity $\epsilon_{\text{eff}}$ of our active random MM, we first calculate the response of the graphene nanoflakes under the effect of optical pumping. Because we assume graphene nanoflakes with dimensions of the order of 30 nm for which quantum
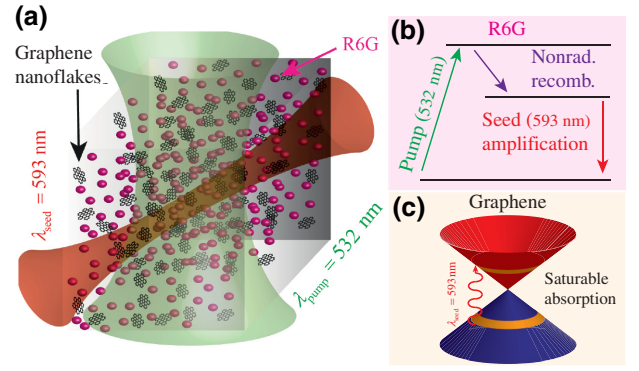


FIG. 1. Sketch of the considered graphene-based active MM consisting of a mixture of graphene nanoflakes and optically pumped R6G molecules embedded in PMMA.

many-body and finite-size effects are negligible [37], we can safely approximate their band structure by the conical band structure of extended graphene around the Dirac points. Furthermore, because unintentional doping of the graphene nanoflakes ($E_F \simeq 0.2$ eV) does not affect significantly $\epsilon_{\text{eff}}$ in the visible, we assume vanishing doping $E_F = 0$. We model electron dynamics in graphene following a previously reported nonperturbative approach in the massless Dirac fermion picture and calculate numerically the intensity-dependent conductivity $\sigma(I)$, where real and imaginary parts are depicted in Fig. 2(a) by the full lines. We find good fitting with the analytical expression [24,30]

$$\sigma(I) = \sigma_0 \left[ \frac{1}{\sqrt{1 + I/I_S}} - i \frac{1 - e^{-\eta_1 \sqrt{I/I_S}}}{\sqrt{1 + \eta_2 (I/I_S)^{0.4}}} \right], \quad (1)$$

where $\sigma_0 = e^2/4\hbar$, $I_S = 137\hbar\omega_S^2\omega_{\text{seed}}^2/(8\pi v_F^2)$, $\omega_S = 6.16$ rad ps$^{-1}$, $\eta_1 = (\omega_\eta/\omega_{\text{seed}})$, $\eta_2 = (\omega_\eta/\omega_{\text{seed}})^{0.8}$, $\omega_\eta = 46.20$ rad ps$^{-1}$, $e$ is the electron charge, $\omega_{\text{seed}} = 2\pi c/\lambda_{\text{seed}}$, $c$ is the speed of light in vacuum, $\hbar$ is the reduced Planck constant, and $v_F \simeq c/300$ is the Fermi velocity of electrons in graphene.

In order to shed light on the effective optical response of the considered active random MM, we assume that the graphene nanoflakes are randomly oriented disks with identical radius $R$. Following a well-established quasistatic approach [27], the optical response of undoped graphene disks is well-reproduced by the first dipolar resonance tail providing the polarizability $\alpha_{\text{gr}} = R^3/[3/(16\epsilon_b) - 2i\epsilon_0 cR/\lambda_{\text{seed}}\sigma(I)]$, which can be approximated by $\alpha_{\text{gr}} \simeq \pi R^2 t_{\text{gr}}\chi_{\text{gr}}$ in the limit $R >> 3\lambda_{\text{seed}}e^2/128\hbar\epsilon_0\epsilon_b c \approx 0.6$ nm, where $\chi_{\text{gr}} = i\sigma(I)/(t_{\text{gr}}\epsilon_0\omega_{\text{seed}})$ is the effective graphene susceptibility. The averaged effective response of the system is calculated by the Clausius-Mossotti effective-medium theory providing

$$\frac{\epsilon_{\text{eff}} - \epsilon_{\text{ext}}}{\epsilon_{\text{eff}} + 2\epsilon_{\text{ext}}} = \frac{(2/3)N_{\text{gr}}\alpha_{\text{gr}}}{3\epsilon_{\text{ext}}}, \quad (2)$$

where $N_{gr}$ is the graphene number density, the factor 2/3 accounts for the random orientation of graphene disks and $\epsilon_{ext} = \epsilon_b + \chi_{R6G}$. In the limit of small graphene density, the Clausius-Mossotti expression reduces to

$$\epsilon_{eff}(I) \simeq \epsilon_b + \chi_{R6G} + (2/3)f_{gr}\chi_{gr}, \qquad (3)$$

where $f_{gr} = N_{gr}\pi R^2 t_{gr}$ is the graphene filling fraction and $t_{gr} = 0.335$ nm is the graphene effective thickness taken from the interlayer distance in graphite. We emphasize that, in the considered regime $\epsilon_{eff}(I)$ does not depend on the geometrical details of the graphene flakes but only on their filling fraction, and in turn our results are robust over the shape and size distributions of the embedded subwavelength inclusions.

Amplification by R6G is modeled by a two-level system, where stable population inversion is assumed to be produced by the external optical pump operating at $\lambda_{pump} = 532$ nm. Because the seed photon is resonant with the two-level transition energy, R6G produces a purely imaginary susceptibility $\chi_{R6G} = -i[g_0(I_{pump})/k_{seed}]/[1 + I/I_S^{R6G}]$, where $k_{seed} = 2\pi/\lambda_{seed}$, $I_S^{R6G} \simeq 150$ MW cm$^{-2}$ is the R6G saturation intensity [38], and $g_0(I_{pump}) \simeq 400$ cm$^{-1}$ is the R6G linear gain coefficient [17] that depends on the R6G density and can be tuned by the external pump. Thus, the effective response of the complex system depicted in Fig. 1 in the limit of small graphene density is accounted by the complex and nonlinear dielectric constant as given in Eq. (3).

We model nonlinear propagation of the monochromatic seed beam with angular frequency $\omega_{seed}$ and carrier wave number $\beta_0 = k_{seed}\sqrt{\epsilon_b}$ by taking the ansatz $\mathbf{E}_{seed}(\mathbf{r}, t) = Re[A(\mathbf{r}_\perp, z)e^{i\beta_0 z - i\omega_{seed}t}\mathbf{n}]$, where $\mathbf{r} = (\mathbf{r}_\perp, z)$ is the position vector, $\mathbf{n}$ is the seed polarization unit vector, and $A(\mathbf{r}_\perp, z)$ is the field envelope. In the slowly varying envelope approximation (SVEA) [39], Maxwell's equations reduce to a generalized Ginzburg-Landau equation [24] for the field envelope

$$i\partial_z A + \frac{1}{2\beta_0}\nabla_\perp^2 A + \frac{\beta_0}{2\epsilon_b}\left[\epsilon_{eff}\left(|A|^2\right) - \epsilon_b\right]A = 0. \qquad (4)$$
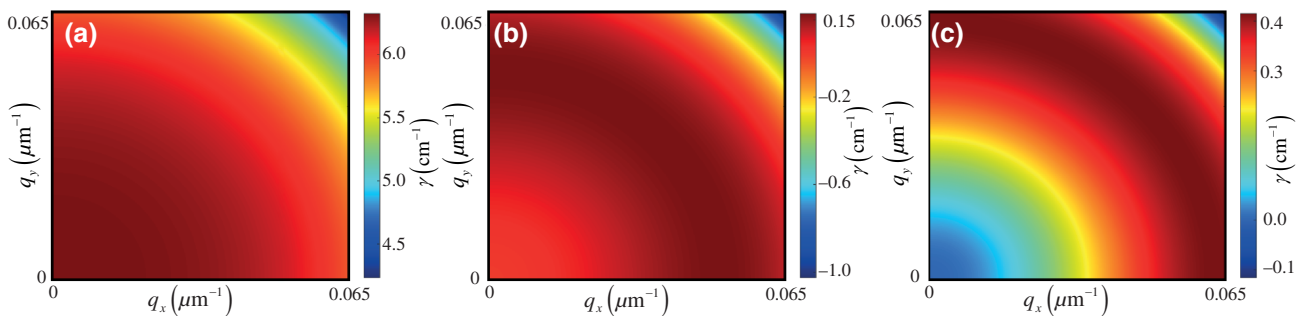


**(a)**

**(b)**
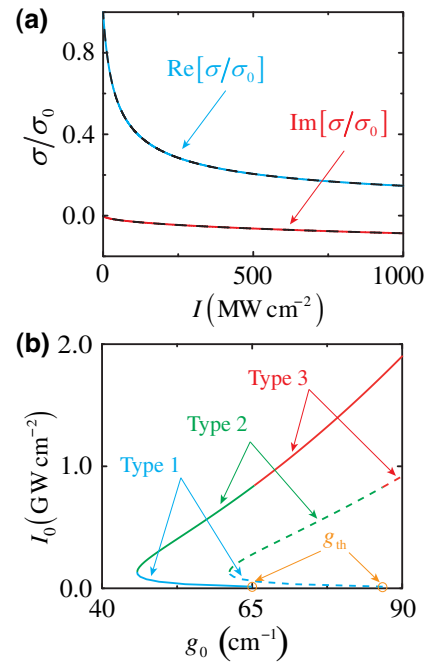
FIG. 2. (a) Dependence of the real ($Re[\sigma/\sigma_0]$, blue line) and imaginary ($Im[\sigma/\sigma_0]$, red line) parts of the nonlinear conductivity $\sigma$ of undoped graphene nanoflakes (normalized to the linear conductivity $\sigma_0$) over the intensity $I$ of seed radiation at $\lambda_{seed} = 593$ nm. Dashed lines indicate fitting with the expression $\sigma(I) = \sigma_0\left[\frac{1}{\sqrt{1+I/I_S}} - i\frac{1-e^{-\eta_1\sqrt{I/I_S}}}{\sqrt{1+\eta_2(I/I_S)^{0.4}}}\right]$. (b) Existence curves of stationary HNWs, where $I_0 = (1/2)\epsilon_0\sqrt{\epsilon_b}c|A_0|^2$ and $g_0$ is the linear gain coefficient for $f = 2.13 \times 10^{-4}$ (full lines) and $f = 2.84 \times 10^{-4}$ (dashed lines). The orange circle dots indicate the background instability threshold $g_{th}$ for the two distinct filling fractions considered.

The nonlinear propagation above accounts for the effects of diffraction, R6G gain, and graphene saturable absorption on the spatial evolution of the seed beam in the effective medium approximation.



FIG. 3. Gain spectrum $\gamma$ (in cm$^{-1}$) of (a) type I for $g_0 = 60$ cm$^{-1}$, (b) type II for $g_0 = 60$ cm$^{-1}$, and (c) type III for $g_0 = 80$ cm$^{-1}$ HNWs, depicting the maximum instability growth rate $\gamma$ as a function of $q_x$ and $q_y$ for $f = 2.13 \times 10^{-4}$.
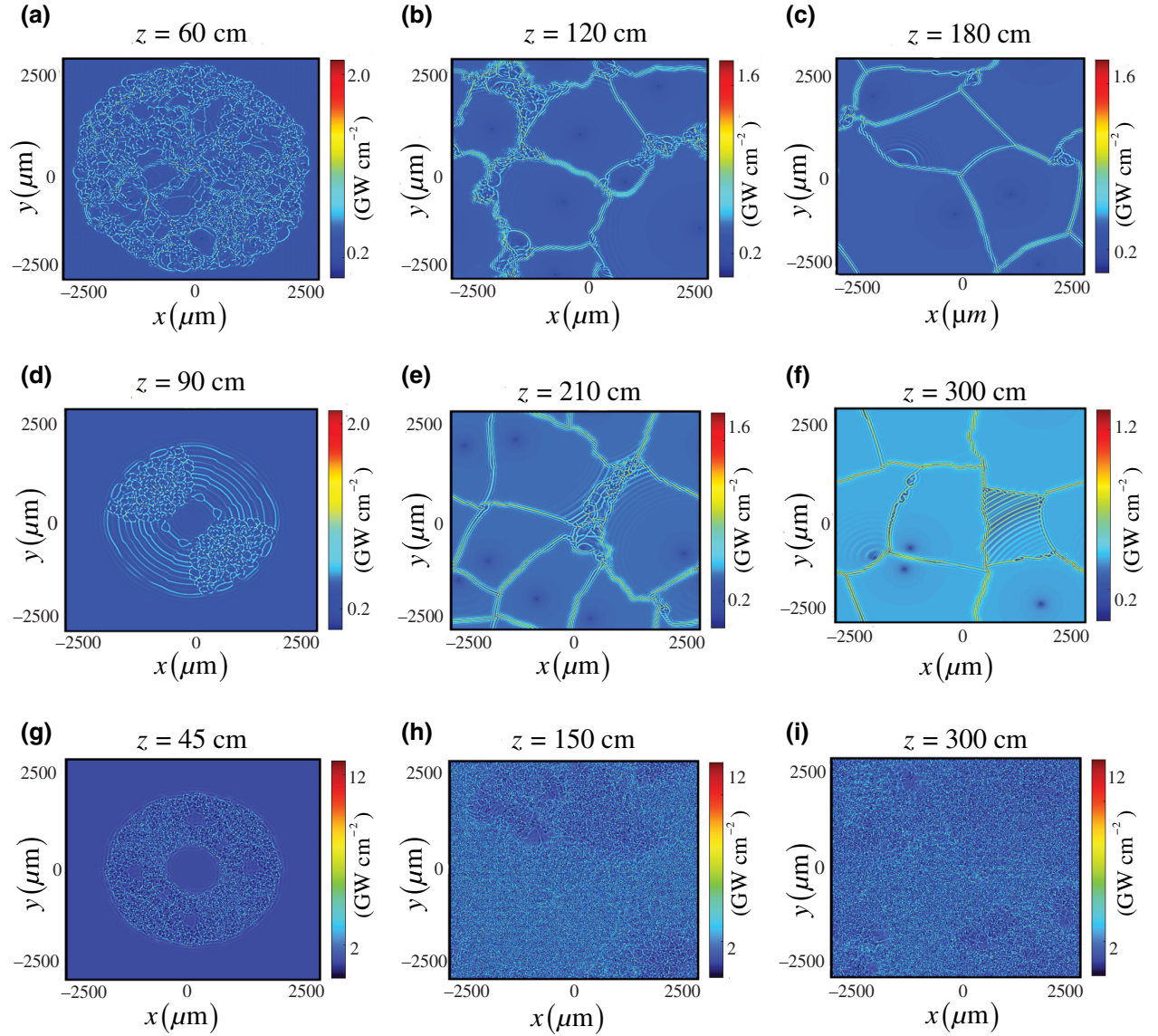
FIG. 4. Evolution of perturbed HNWs of (a)–(c) type I ($g_0 = 60$ cm$^{-1}$), (d)–(f) type II ($g_0 = 60$ cm$^{-1}$), and (g)–(i) type III ($g_0 = 80$ cm$^{-1}$) for $f = 2.13 \times 10^{-4}$. The density plots depict the dependence of the intensity profile $I(\mathbf{r}_\perp)$ over the transverse position vector $\mathbf{r}_\perp = x\hat{e}_x + y\hat{e}_y$ for several distinct propagation distances $z = \bar{z}$ indicated at the top of every figure.

## III. NONLINEAR WAVES

### A. Homogeneous nonlinear waves (HNWs)

Extended HNWs are excited by a seed plane wave where the input envelope does not depend on the transverse position $A(\mathbf{r}_\perp, 0) = A_0$. We calculate the nonlinear dispersion of stationary HNWs by taking the ansatz $A(z) = A_0 e^{i\delta\beta z}$ in Eq. (4) suppressing the diffraction term $\nabla_\perp^2 A = 0$ and obtaining the propagation constant correction $\delta\beta = (\beta_0/2\epsilon_b)\left\{\text{Re}\left[\epsilon_{\text{eff}}\left(|A_0|^2\right)\right] - \epsilon_b\right\}$. Conversely to Hamiltonian systems where $A_0$ is arbitrary, owing to dissipation (accounted by $\text{Im}\epsilon_{\text{eff}}$) stationary HNWs exist only for specific input amplitudes $A_0$ fixed by the nonlinear condition $\text{Im}[\epsilon_{\text{eff}}\left(|A_0|^2\right)] = 0$, which we solve by

the Newton-Raphson method for several distinct values of the linear gain coefficent $g_0$. Thanks to graphene saturable absorption, we observe a subcritical bifurcation from the background $A_0 = 0$ at a specific gain threshold $g_{\text{th}}$ depending on the graphene filling fraction $f$ and leading to bistability of two distinct solutions for $g_0 < g_{\text{th}}$, which we name type I and II, as illustrated in Fig. 2(b). Conversely, for $g_0 > g_{\text{th}}$ we find only one homogenous solution, which we name type III, see Fig. 2(b).

### B. Modulational instability of HNWs

The stability of HNWs against small-amplitude perturbing waves with amplitudes $\delta A_1$, $\delta A_2$ and wave vector $\mathbf{q}_\perp$ is
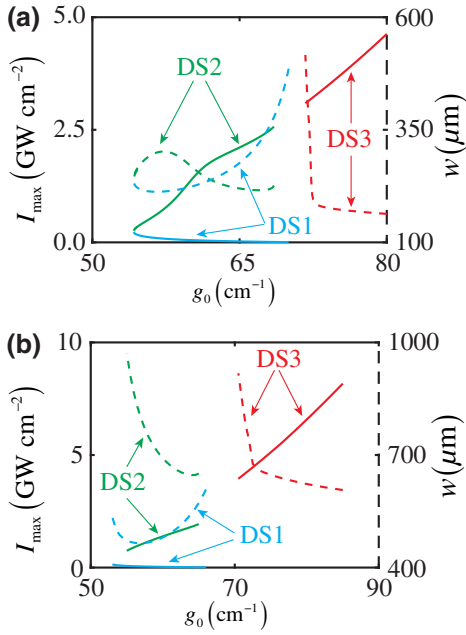
FIG. 5. Dependence over the linear gain coefficient $g_0$ of peak intensities $I_{max}$ (full lines, left full vertical axis) and spot sizes $w$ (dashed lines, right dashed vertical axis) of the numerically calculated DSs with topological charge (a) $m = 0$ and (b) $m = 1$ for graphene filling fraction $f = 2.13 \times 10^{-4}$.
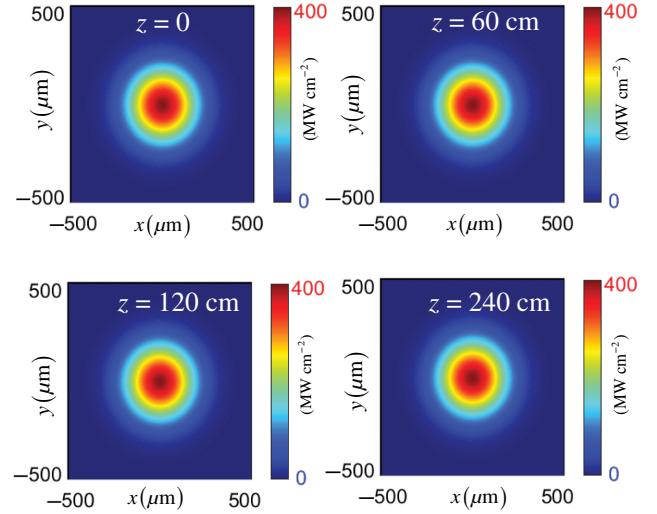
FIG. 6. Density plots illustrating the dependence of the intensity profiles $I(\mathbf{r}_\perp, \bar{z})$ of the stable $m = 0$ DS2 (for $g_0 = 55$ cm$^{-1}$ and $f = 2.13 \times 10^{-4}$) over $\mathbf{r}_\perp = x\hat{e}_x + y\hat{e}_y$ and stationary propagation at several distinct $z = \bar{z}$ indicated on top of every plot.

evaluated by setting

$$A = A_0 + \left[\delta A_1 e^{hz + i\mathbf{q}_\perp \cdot \mathbf{r}_\perp} + \delta A_2^* e^{h^* z - i\mathbf{q}_\perp \cdot \mathbf{r}_\perp}\right] e^{i\delta\beta z}, \quad (5)$$

where $h = \gamma + i\Upsilon$, $\gamma$ and $\Upsilon$ are the instability growth rate and the wave-number shift, respectively, induced by the perturbing waves. Inserting this expression in Eq. (4), and linearizing with respect to the small amplitudes $\delta A_1, \delta A_2$, we find

$$\begin{bmatrix} -iF_1 + iF_2 & i\delta_2 F' A_0^2 \\ -i\delta_2 F'^* A_0^{2*} & iF_1 + iF_2^* \end{bmatrix} \begin{bmatrix} \delta A_1 \\ \delta A_2 \end{bmatrix} = h \begin{bmatrix} \delta A_1 \\ \delta A_2 \end{bmatrix}, \quad (6)$$

where, $\delta_2 = (2\beta_0)^{-1}$, $F = (\beta_0/2\epsilon_b)\left[\epsilon_{eff}(|A_0|^2) - \epsilon_b\right]$, $F' = \partial_{|A_0|^2} F$, $F_1 = \delta\beta + \delta_2 q_\perp^2$ and $F_2 = \delta_2(F'|A_0|^2 + F)$.

We calculate numerically the complex eigenvalues $h = \gamma + i\Upsilon$ of such a linear algebraic system of equations for every wave vector $\mathbf{q}_\perp$. Positive and negative growth rates $\gamma$ indicate instability and stability against small-amplitude perturbations. We find that all HNWs are unstable and that, while the maximum instability growth rate $\gamma$ is peaked at $q_\perp = 0$ for type II HNWs, see Fig. 3(a), for type II and type III HNWs it is peaked at a specific $q_\perp = \bar{q}_\perp$, see Figs. 3(b) and 3(c). This suggests that perturbed HNWs can develop filamentation over propagation. Furthermore, we evaluate the stability of the background $A_0 = 0$, finding that it is stable for $g_0 < g_{th}$ and unstable for $g_0 > g_{th}$. In turn, $g_{th}$ represents the linear gain stability threshold of the background. Owing to the above described

modulational instability scenario, nonlinear dynamics in subcritical and overcritical domains leads to qualitatively different phenomena. In order to gain insight on the evolution of perturbed HNWs, we solve Eq. (4) in propagation by the split-step discrete Fourier transform complemented with a fourth-order Runge-Kutta algorithm, with results summarized in Fig. 4, where we depict the intensity profile $I(\mathbf{r}_\perp, \bar{z}) = (1/2)\epsilon_0\sqrt{\epsilon_b}c|A(\mathbf{r}_\perp, \bar{z})|^2$ as a function of $\mathbf{r}_\perp$ for (a)–(c) type I ($g_0 = 60$ cm$^{-1}$), (d)–(f) type II ($g_0 = 60$ cm$^{-1}$), and (g)–(i) type III ($g_0 = 80$ cm$^{-1}$) perturbed HNWs for $f = 2.13 \times 10^{-4}$ at several distinct propagation distances $z = \bar{z}$. Note that for $g_0 = 60$ cm$^{-1}$ [subcritical since $g_0 < g_{th}$, see Fig. 1(b)] both type I and type II HNWs develop instabilities over propagation and tend to filament into self-organized patterns and interacting domains, while for $g_0 = 80$ cm$^{-1}$ [overcritical since $g_0 > g_{th}$, see Fig. 1(b)] the dynamics becomes chaotic [40].

## C. Localized NWs

Localized, stationary, and self-sustaining nonlinear waves, commonly named dissipative solitons [2], are calculated by setting the ansatz $A(\mathbf{r}_\perp, z) = A_0(r_\perp)e^{i\delta\beta z + im\phi}$ in Eq. (4), where $m$ is an arbitrary topological charge and $\phi$ is the azimuthal angle between $\mathbf{r}_\perp$ and the $x$ axis, obtaining an ordinary differential equation (ODE) for $A_0(r_\perp)$,

$$-\delta\beta A_0(r_\perp) + \frac{1}{2\beta_0}\left[\frac{1}{r_\perp}\frac{d}{dr_\perp}\left(r_\perp\frac{dA_0}{dr_\perp}\right) - \frac{m^2}{r_\perp^2}A_0\right] +$$

$$+ \frac{\beta_0}{2\epsilon_b}\{\epsilon_{eff}\left[|A_0(r_\perp)|^2\right] - \epsilon_b\}A_0(r_\perp) = 0. \quad (7)$$
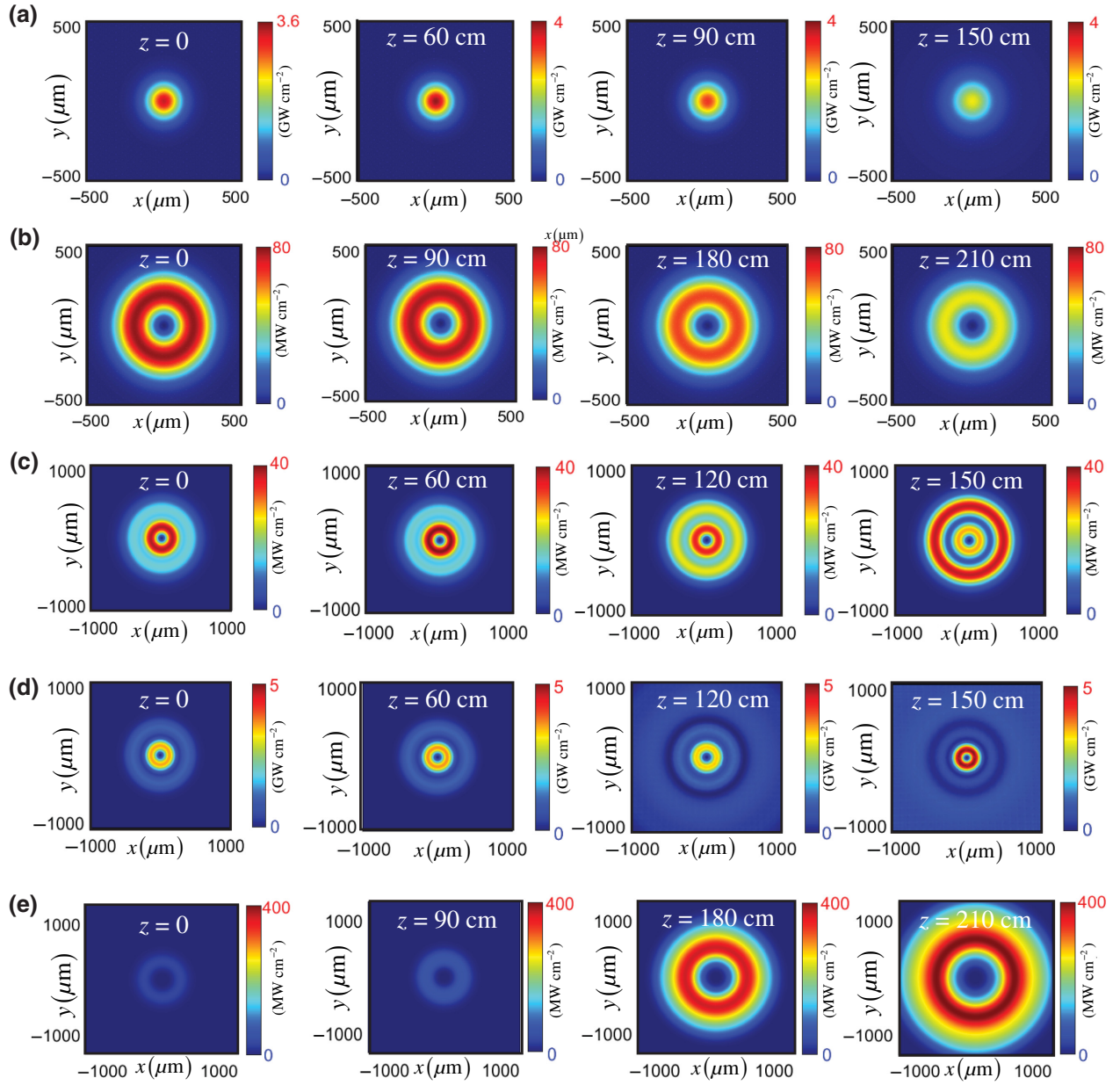
FIG. 7. Density plots illustrating the dependence of the intensity profiles $I(\mathbf{r}_\perp, \bar{z})$ over $\mathbf{r}_\perp = x\hat{e}_x + y\hat{e}_y$ of (a) $m = 0$ DS3 for $g_0 = 75$ cm$^{-1}$, (b) $m = 1$ DS1 for $g_0 = 55$ cm$^{-1}$, (c) $m = 1$ DS2 for $g_0 = 60$ cm$^{-1}$, (d) $m = 1$ DS3 for $g_0 = 75$ cm$^{-1}$, and (e) $m = 2$ DS2 for $g_0 = 60$ cm$^{-1}$ at several distinct $z = \bar{z}$ indicated on top of every plot. In all plots the graphene filling fraction is set to $f = 2.13 \times 10^{-4}$.

In order to solve the ODE above, we transform it into a nonlinear system of algebraic equations by discretizing the spatial variable $r_\perp(n) = r_n$, first-order $dA_0/dr_\perp = [A_0(r_{n+1}) - A_0(r_n)]/(r_{n+1} - r_n)$ and second-order $d^2A_0/dr_\perp^2 = [A_0(r_{n-1}) - 2A_0(r_n) + A_0(r_{n+1})]/(r_n - r_{n-1})^2$ derivatives with $n = 1, 2, ..., N$ and by applying the homogeneous boundary conditions $A_0(r_1) = A_0(r_2)$ and $A(r_N) = 0$. We solve the resulting nonlinear system of algebraic equations numerically through the Newton-Raphson method. Also for localized NWs, we observe a subcritical bifurcation from the trivial vacuum

$A_0(\mathbf{r}_\perp) = 0$ and we find three types of localized stationary solutions (DS1, DS2, DS3) for every $m = 0, 1, 2$. In Figs. 5(a) and 5(b) we plot the maximum intensity $I_{\max} = (1/2)\epsilon_0\sqrt{\epsilon_b}c \max|A_0(\mathbf{r}_\perp)|^2$ (full lines) and the spot size $w = 2[\int_0^{+\infty} r_\perp^3 |A_0(\mathbf{r}_\perp)|^2 dr_\perp / \int_0^{+\infty} r_\perp |A_0(\mathbf{r}_\perp)|^2 dr_\perp]^{1/2}$ (dashed lines) of (a) $m = 0$ and (b) $m = 1$ DSs (of types 1, 2, 3) against $g_0$ for fixed graphene filling fraction $f = 2.13 \times 10^{-4}$. Similarly to HNWs, also for localized NWs DS1 and DS2 coexist in the bistable subcritical domain, while DS3 exists only in the overcritical domain. All the intensity profiles of the DSs found are bell shaped, while
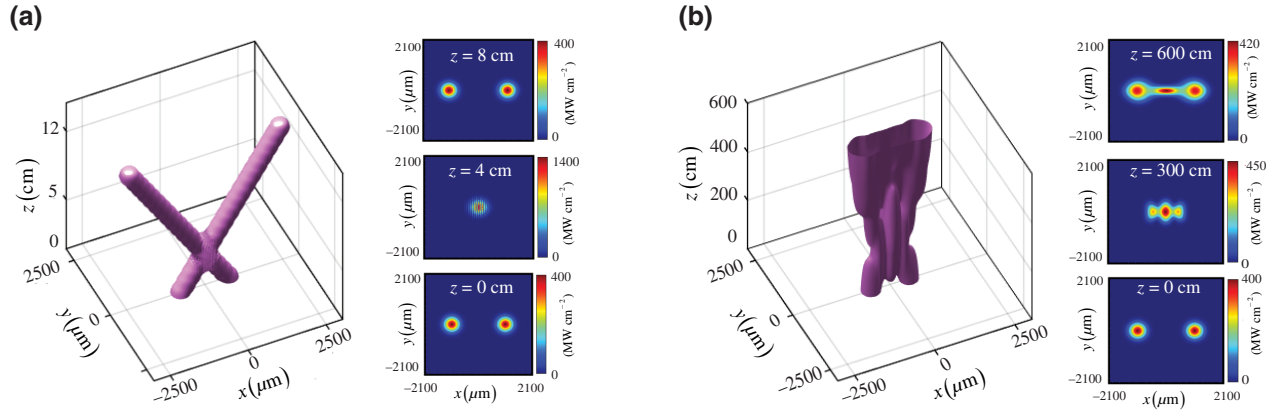
FIG. 8. Collision dynamics of two stable $m = 0$ DS2s for $g_0 = 55$ cm$^{-1}$ with initial separation $2r_0 = 2000$ $\mu$m and collision angle (a) $\theta = 2°(> \theta_c \approx 0.05°)$ and (b) $\theta = 0.02°(< \theta_c \approx 0.05°)$. The main figures show the three-dimensional intensity isosurface $I = 50$ MW cm$^{-2}$, while the insets depict the spatial profile of the intensity distribution (in the $x$-$y$ plane) at distinct propagation distances indicated on top of every subplot.

their phase $\varphi(\mathbf{r}_\perp) = \text{atan}[\text{Im}A_0(\mathbf{r}_\perp)/\text{Re}A_0(\mathbf{r}_\perp)]$ is not uniform over the $x$-$y$ plane, which implies an internal power flow enabling stationary propagation of DSs [2]. Indeed, note that in the considered dissipative system, conversely to traditional soliton families in Hamiltonian systems, for every DS type there exists only one solution with fixed peak intensity and spot size, which arises from the double nonlinear compensation of diffraction versus focusing and gain versus absorption [2]. Note also that both the peak intensity $(0 < I_{\text{max}} < 10$ GW cm$^{-2})$ and the spot size $(100 \ \mu\text{m} \ < w < 101$ mm$)$ of every DS can be tuned efficiently by the pump intensity $I_{\text{pump}}$ modulating the linear gain coefficient $50$ cm$^{-1} < g_0(I_{\text{pump}}) < 90$ cm$^{-1}$, which is experimentally attainable with R6G [17].

## IV. DISCUSSION

In order to shed light on radiation dynamics in the complex system considered, we investigate the stability of the found DSs for $m = 0, 1, 2$ in propagation by solving Eq. (4) through a split-step discrete Fourier transform complemented with a fourth-order Runge-Kutta algorithm. We find that stability occurs only for $m = 0$ DS2 in the subcritical domain, which intensity profile and stationary propagation is illustrated in Fig. 6, while all the other DSs found ($m = 0$ DS1,3 and $m = 1, 2$ DS1-3) are unstable. In Fig. 7 we illustrate the initial steps of the unstable dynamics of (a) $m = 0$ DS3 for $g_0 = 75$ cm$^{-1}$, (b) $m = 1$ DS1 for $g_0 = 55$ cm$^{-1}$, (c) $m = 1$ DS2 for $g_0 = 60$ cm$^{-1}$, (d) $m = 1$ DS3 for $g_0 = 75$ cm$^{-1}$, and $m = 2$ DS2 for $g_0 = 60$ cm$^{-1}$. In all plots the graphene filling fraction is set to $f = 2.13 \times 10^{-4}$. Due to the instability of the background and the existence of several unstable DSs, propagation over longer distances becomes chaotic in the overcritical domain. Conversely, propagation of azimuthally perturbed DSs over longer distances in the subcritical

domain leads to filamentation into several stable $m = 0$ DS2 solitons, see the Videos within the Supplemental Material [41], where we illustrate the breaking of $m = 1$ and $m = 2$ DSs into two and four repulsive $m = 0$ DSs, respectively.

In order to study the collision dynamics, we perform extensive numerical simulations launching identical localized stable DS pairs (with $m = 0$) in the ($x$-$y$) plane. We simulate Eq. (4) with initial condition at $z = 0$ given by

$$A_{\text{in}} = \sum_{s=\pm 1} A_0(r_\perp + sr_0)e^{im\phi}e^{is\theta x}, \qquad (8)$$

where $2\theta$ is the collision angle, $2r_0$ is the separation between the centers of the identical solitons and $A_0$ is the DS2 solution obtained by solving the ODE of Eq. (7). We launch the solitons such that at $z = 0$ their centers lie entirely on the $x$ axis. In Fig. 8 we illustrate the collision dynamics for two distinct collision angles showing that for a collision angle $\theta > \theta_c \approx 0.05°$ the DS pair undergoes an elastic collision consistent with the result reported in Refs. [42,43], highlighting the particlelike nature of DSs, see Fig. 8(a). However, we find that when $\theta < \theta_c \approx 0.05°$ the soliton pair breaks into multiple localized spots, see Fig. 8(b). Over longer propagation, we observe alternate repulsion and attraction between the multiple DSs generated, leading to a complex interaction dynamics.

## V. CONCLUSIONS

In conclusion, we describe the spatial formation of dissipative nonlinear waves in a graphene-based active random metamaterial composed of randomly dispersed graphene nanoflakes and optically pumped R6G. Owing to bistability of HNWs in a subcritical region below the

instability threshold of the background, there exist several DS vortices with distinct topological charges. By investigating systematically the existence and stability of DSs one finds that only one specific DS with vanishing topological charge is stable in the subcritical domain and becomes unstable in the overcritical domain. Analysis of propagation dynamics of perturbed HNWs and DSs indicates that nonlinear waves break into stable and repulsive DSs with fixed topological charge $m = 0$. This indicates that graphene-based active random metamaterials enable the control of mode operation since the spatial pattern of the excited nonlinear waves is fixed by the density of graphene nanoflakes and the external optical pump tuning the linear gain coefficient $g_0$. Our results indicate that self-organization of coherent radiation structures in disordered systems can be exploited to design cavity-free laser operation and amplification, opening alternative possibilities for the advancement of random lasers.

## ACKNOWLEDGMENTS

[1] Dissipative Solitons: From Optics to Biology and Medicine, edited by N. Akhmediev and A. Ankiewicz, Lecture Notes in Physics, Vol. 751 (Springer, Berlin, 2008).

[2] P. Grelu and N. Akhmediev, Dissipative solitons for mode-locked lasers, Nat. Photonics **6**, 84 (2012).

[3] J. Peng, S. Boscolo, Z. Zhao, and H. Zeng, Breathing dissipative solitons in mode-locked fiber lasers, Sci. Adv. **5**, eaax1110 (2019).

[4] O. B. Helgason, F. R. Arteaga-Sierra, Z. Ye, K. Twayana, P. A. Andrekson, M. Karlsson, J. Schröder, and V. Torres-Company, Dissipative solitons in photonic molecules, Nat. Photonics **15**, 305 (2021).

[5] S. Yanchuk, S. Ruschel, J. Sieber, and M. Wolfrum, Temporal Dissipative Solitons in Time-Delay Feedback Systems, Phys. Rev. Lett. **123**, 053901 (2019).

[6] E. A. Ostrovskaya, J. Abdullaev, A. S. Desyatnikov, M. D. Fraser, and Y. S. Kivshar, Dissipative solitons and vortices in polariton Bose-Einstein condensates, Phys. Rev. A **86**, 013636 (2012).

[7] V. A. Brazhnyi, V. V. Konotop, V. M. Pérez-García, and H. Ott, Dissipation-Induced Coherent Structures in Bose-Einstein Condensates, Phys. Rev. Lett. **102**, 144101 (2009).

[8] E. Tesio, G. R. M. Robb, T. Ackemann, W. J. Firth, and G.-L. Oppo, Dissipative solitons in the coupled dynamics of light and cold atoms, Opt. Express **21**, 26144 (2013).

[9] Y. Song, X. Shi, C. Wu, D. Tang, and H. Zhang, Recent progress of study on optical solitons in fiber lasers, Appl. Phys. Rev. **6**, 021313 (2019).

[10] E. A. Ultanir, G. I. Stegeman, D. Michaelis, C. H. Lange, and F. Lederer, Stable Dissipative Solitons in Semiconductor Optical Amplifiers, Phys. Rev. Lett. **90**, 253903 (2003).

[11] D. S. Wiersma, The physics and applications of random lasers, Nat. Phys. **4**, 359 (2008).

[12] S. Gottardo, R. Sapienza, P. D. García, A. Blanco, D. S. Wiersma, and C. López, Resonance-driven random lasing, Nat. Photonics **2**, 429 (2008).

[13] D. S. Wiersma, Disordered photonics, Nat. Photonics **7**, 188 (2013).

[14] D. J. Bergman and M. I. Stockman, Surface Plasmon Amplification by Stimulated Emission of Radiation: Quantum Generation of Coherent Surface Plasmons in Nanosystems, Phys. Rev. Lett. **90**, 027402 (2003).

[15] M. A. Noginov, G. Zhu, A. M. Belgrave, R. Bakker, V. M. Shalaev, E. E. Narimanov, S. Stout, E. Herz, T. Suteewong, and U. Wiesner, Demonstration of a spaser-based nanolaser, Nature **460**, 1110 (2009).

[16] M. I. Stockman, The spaser as a nanoscale quantum generator and ultrafast amplifier, J. Opt. **12**, 024004 (2010).

[17] M. A. Noginov, G. Zhu, M. Mayy, B. A. Ritzo, N. Noginova, and V. A. Podolskiy, Stimulated Emission of Surface Plasmon Polaritons, Phys. Rev. Lett. **101**, 226806 (2008).

[18] A. Marini, A. V. Gorbach, D. V. Skryabin, and A. V. Zayats, Amplification of surface plasmon polaritons in the presence of nonlinearity and spectral signatures of threshold crossover, Opt. Lett. **34**, 2864 (2009).

[19] P. M. Bolger, W. Dickson, A. V. Krasavin, L. Liebscher, S. G. Hickey, D. V. Skryabin, and A. V. Zayats, Amplified spontaneous emission of surface plasmon polaritons and limitations on the increase of their propagation length, Opt. Lett. **35**, 1197 (2010).

[20] I. De Leon and P. Berini, Amplification of long-range surface plasmons by a dipolar gain medium, Nat. Photonics **4**, 382 (2010).

[21] N. I. Zheludev, S. L. Prosvirnin, N. Papasimakis, and V. A. Fedotov, Lasing spaser, Nat. Photonics **2**, 351 (2008).

[22] O. Hess, J. B. Pendry, S. A. Maier, R. F. Oulton, J. M. Hamm, and K. L. Tsakmakidis, Active nanoplasmonic metamaterials, Nat. Mater. **11**, 573 (2012).

[23] A. Marini and F. J. García de Abajo, Self-organization of frozen light in near-zero-index media with cubic nonlinearity, Sci. Rep. **6**, 20088 (2016).

[24] A. Marini and F. J. García de Abajo, Graphene-Based Active Random Metamaterials for Cavity-Free Lasing, Phys. Rev. Lett. **116**, 217401 (2016).

[25] F. Bonaccorso, Z. Sun, T. Hasan, and A. C. Ferrari, Graphene photonics and optoelectronics, Nat. Photon. **4**, 611 (2010).

[26] Q. Bao and K. P. Loh, Graphene photonics, plasmonics, and broadband optoelectronic devices, ACS Nano **6**, 3677 (2012).

[27] F. J. García de Abajo, Graphene plasmonics: Challenges and opportunities, ACS Photon. **1**, 135 (2014).

[28] Q. Bao, H. Zhang, Y. Wang, Z. Ni, Y. Yan, Z. X. Shen, K. P. Loh, and D. Y. Tang, Atomic-Layer graphene as a saturable absorber for ultrafast pulsed lasers, Adv. Funct. Mater. **19**, 3077 (2009).

[29] G. Xing, H. Guo, X. Zhang, T. C. Sum, and C. H. A. Huan, The physics of ultrafast saturable absorption in graphene, Opt. Express **18**, 4564 (2010).

[30] A. Marini, J. D. Cox, and F. J. García de Abajo, Theory of graphene saturable absorption, Phys. Rev. B **95**, 125408 (2017).

[31] B. Guo, Q. Xiao, S. Wang, and H. Zhang, 2D layered materials: Synthesis, nonlinear optical properties, and device applications, Laser Photonics Rev. **13**, 1800327 (2019).

[32] J. Shi, Z. Li, D. Sang, Y. Xiang, J. Li, S. Zhang, and H. Zhang, THz photonics in two dimensional materials and metamaterials: Properties, devices and prospects, J. Mater. Chem. c **6**, 1291 (2018).

[33] Y. Xiang, X. Dai, J. Guo, H. Zhang, S. Wen, and D. Tang, Critical coupling with graphene-based hyperbolic metamaterials, Sci. Rep. **4**, 5483 (2014).

[34] M. Leonetti, C. Conti, and C. Lopez, Switching and amplification in disordered lasing resonators, Nat. Commun. **4**, 1740 (2013).

[35] M. Yi and Z. Shen, A review on mechanical exfoliation for scalable production of graphene, J. Mater. Chem. A **00**, 1 (2012).

[36] Y. Zhang, L. Zhang, and C. Zhou, Review of chemical vapor deposition of graphene and related applications, Acc. Chem. Res. **46**, 2329 (2013).

[37] J. D. Cox and F. J. García de Abajo, Electrically tunable nonlinear plasmonics in graphene nanoislands, Nat. Commun. **5**, 5725 (2014).

[38] B. Nithyaja, H. Misha, P. Radhakrishnan, and V. P. N. Nampoor, Effect of deoxyribonucleic acid on nonlinear optical properties of Rhodamine 6G-polyvinyl alcohol solution, Appl. Phys. Lett. **109**, 023110 (2011).

[39] M. Leonetti, C. Conti, and C. Lopez, Non-locality and collective emission in disordered lasing resonators, Light Sci. Appl. **2**, e88 (2013).

[40] A. Marini and D. V. Skryabin, Ginzburg-Landau equation bound to the metal-dielectric interface and transverse nonlinear optics with amplified plasmon polaritons, Phys. Rev. A **81**, 033850 (2010).

[41] See Supplemental Material at http://link.aps.org/supplemental/10.1103/PhysRevApplied.17.044036 for videos describing the propagation of azimuthally perturbed $m = 1$ and $m = 2$ DSs in the subcritical domain.

[42] M. Shih and M. Segev, Incoherent collisions between two-dimensional bright steady-state photorefractive spatial screening solitons, Opt. Lett. **22**, 1538 (1996).

[43] Z. H. Musslimani, M. Soljacic, M. Segev, and D. N. Christodoulides, Interactions between two-dimensional composite vector solitons carrying topological charges, Phy. Rev. E **63**, 066608 (2001).